

Serum Dyslipidemia Is Induced by Internal Exposure to Strontium-90 in Mice, Lipidomic Profiling Using a Data-Independent Liquid Chromatography–Mass Spectrometry Approach

Maryam Goudarzi,^{*,†} Waylon M. Weber,[‡] Juijung Chung,[†] Melanie Doyle-Eisele,[‡] Dunstana R. Melo,[‡] Tytus D. Mak,[§] Steven J. Strawn,[†] David J. Brenner,[⊥] Raymond Guilmette,[‡] and Albert J. Fornace Jr.^{†,¶}

[†]Department of Biochemistry and Molecular & Cellular Biology, Georgetown University, 3970 Reservoir Rd. NW, Washington, D.C. 20057, United States

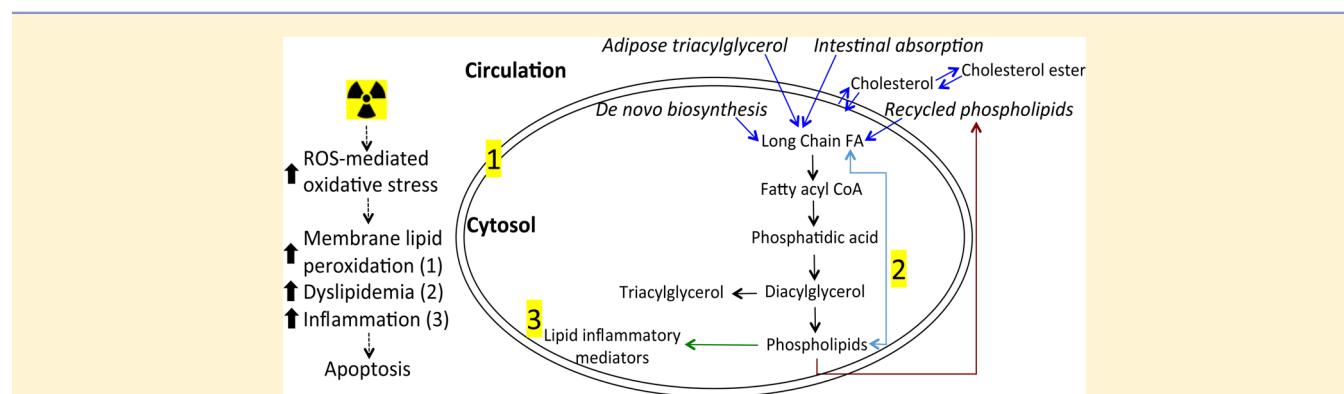
[‡]Lovelace Respiratory Research Institute, 2425 Ridgecrest Dr. SE, Albuquerque, New Mexico 87108, United States

[§]Mass Spectrometry Data Center, National Institute of Standards and Technology, 100 Bureau Drive, Gaithersburg, Maryland 20899, United States

[⊥]Center for Radiological Research, Columbia University, 630 West 168th Street, VC11-240, New York, New York 10032, United States

[¶]Lombardi Comprehensive Cancer Center, Georgetown University, Washington, D.C. 20057, United States

Supporting Information



ABSTRACT: Despite considerable research into the environmental risks and biological effects of exposure to external beam γ rays, incorporation of radionuclides has largely been understudied. This dosimetry and exposure risk assessment is challenging for first responders in the field during a nuclear or radiological event. Therefore, we have developed a workflow for assessing injury responses in easily obtainable biofluids, such as urine and serum, as the result of exposure to internal emitters cesium-137 (^{137}Cs) and strontium-90 (^{90}Sr) in mice. Here we report on the results of the untargeted lipidomic profiling of serum from mice exposed to ^{90}Sr . We also compared these results to those from previously published ^{137}Cs exposure to determine any differences in cellular responses based on exposure type. The results of this study conclude that there is a gross increase in the serum abundance of triacylglycerides and cholesterol esters, while phosphatidylcholines and lysophosphatidylcholines displayed decreases in their serum levels postexposure at study days 4, 7, 9, 25, and 30, with corresponding average cumulative skeleton doses ranging from 1.2 ± 0.1 to 5.2 ± 0.73 Gy. The results show significant perturbations in serum lipidome as early as 2 days postexposure persisting until the end of the study (day 30).

KEYWORDS: strontium-90, internal emitter, radiation exposure, lipidomics, UPLC, data-independent mass spectrometry, phospholipid, triacylglycerol

INTRODUCTION

The modern world has seen an increase in the use of nuclear energy in medicine and industry. While important, nuclear plants pose an environmental risk and a radiation hazard to the nearby populations. More recently, this technology has been of great concern if used in an improvised nuclear device. With two major nuclear disasters in recent history, Chernobyl and Fukushima, and with increasing threats of a nuclear or

radiological attack, our group has taken important steps in establishing robust radiation exposure markers in easily accessible biofluids. Urine and blood may be used in the early medical response and management of victims of a nuclear or radiological disaster to determine exposure, radiation dose,

Received: June 23, 2015

Published: August 11, 2015

Table 1. Experimental Details^a

group	injection dose	in vivo counts (~days)	necropsy (days)	average committed skeleton dose	standard deviation	dose coefficient
control	vehicle	N/A	4	N/A	N/A	N/A
control	vehicle	N/A	7	N/A	N/A	N/A
control	vehicle	N/A	9	N/A	N/A	N/A
control	vehicle	N/A	25	N/A	N/A	N/A
control	vehicle	N/A	30	N/A	N/A	N/A
strontium	2.10×10^{-5} Bq	0–4	4	1.2 Gy	± 0.10	5.66×10^{-6} (Gy.Bq ⁻¹)
strontium	2.06×10^{-5} Bq	0–7	7	1.8 Gy	± 0.12	8.79×10^{-6} (Gy.Bq ⁻¹)
strontium	1.98×10^{-5} Bq	0–7, 9	9	2.1 Gy	± 0.32	1.07×10^{-5} (Gy.Bq ⁻¹)
strontium	2.04×10^{-5} Bq	0–7, 9, 12, 16, 20, 25	25	4.8 Gy	± 0.39	2.34×10^{-5} (Gy.Bq ⁻¹)
strontium	1.96×10^{-5} Bq	0–7, 9, 12, 16, 20, 25, 27, 30	30	5.2 Gy	± 0.73	2.68×10^{-5} (Gy.Bq ⁻¹)

^aThe strontium exposed and the control groups were matched based on necropsy day, which was decided to achieve the specified skeleton doses in the “average skeleton dose” column. There were eight mice per each strontium-exposed and control group. N/A, not applicable.

and subsequent risk during patient triage. We have extensively studied the effects of external beam irradiation in vivo^{1–4} as well as the effects of internal exposure to internal emitters such as cesium-137 (¹³⁷Cs)^{5,6} and strontium-90 (⁹⁰Sr).⁷ Exposure to internal emitters in the fallout of a nuclear disaster is a major health concern due to their environmental persistence and the significant temporal and spatial differences in radiation dose patterns. Because only limited information was available on in vivo exposure to internal emitters, we set out to study the urinary and serum perturbations induced by internal exposure to ¹³⁷Cs in mice over the course of 30 days. These results showed a shift in energy metabolism and changes in the lipid metabolism, particularly membrane phospholipids.⁵ In continuation of our efforts into the effects of exposure to internal emitters, we looked at ⁹⁰Sr. This radionuclide, along with ¹³⁷Cs, is considered one of the most important fission product radionuclides because of its relatively long physical half-time (about 30 years). Because of its placement in Group II of the periodic table, ⁹⁰Sr can chemically replace calcium in the bone mineral and remain there for long periods of time. ⁹⁰Sr and its radioactive decay product ⁹⁰Y are pure beta-emitting radionuclides; unlike γ radiation, beta decay is less penetrating and leads to a more nonuniform irradiation of tissues. The urinary metabolomic analysis of mice exposed to ⁹⁰Sr recently showed that although some of the long-established IR (ionizing radiation) markers, such as citric acid and taurine, were among the most statistically significant markers of ⁹⁰Sr exposure, the urinary metabolomic profile of the ⁹⁰Sr-exposed mice was unique. In particular, butanoate and vitamin B metabolisms were determined to be central to other metabolic perturbations including the tricarboxylic acid (TCA) cycle.⁷ Our current study focuses on the serum lipidomic phenotype of the same ⁹⁰Sr-exposed mice, which will be followed by an in-depth serum metabolomic analysis to provide a window into the serum lipidome and metabolome as the result of internal exposure to ⁹⁰Sr.

The current serum lipidomic study in mice exposed to ⁹⁰Sr was based on a previously established lipidomic workflow using ultraperformance liquid chromatography coupled with quadrupole time-of-flight mass spectrometry (UPLC-QToFMS) in a data-independent mode.⁵ The serum samples collected at different time points post ⁹⁰Sr exposure, day 4, 7, 9, 25, and 30, were used at the calculated cumulative average skeleton doses of 1.2 ± 0.10 Gy, 1.8 ± 0.12 Gy, 2.1 ± 0.32 Gy, 4.8 ± 0.39 Gy, 5.2 ± 0.73 Gy, respectively. The radiation dose rate in this study varied from 0.21–0.12 mGy/min by the end of the study.

However, an important factor in dosimetry, studying the effects of variable, decreasing in this case, dose rate on the end points was beyond the scope of this study. Moreover, internal emitters continue to irradiate the cells and tissues during the course of the study, which accounts for a different dose pattern than with external irradiation, for example, with X-rays, which are typically delivered externally in one very brief exposure. While we recognize these important factors, our objective was to establish a robust serum lipidomic signature for ⁹⁰Sr in mice. The results of this study and our previous work will be useful in gaining insight into the biological and cellular mechanisms that undergo significant perturbations as the result of exposure due to intake of radionuclides compared to external beam γ -rays and X-rays.

MATERIALS AND METHODS

The following internal standards were obtained from Avanti Polar Lipids (Alabaster, AL): sphingolipid mix (SM) II, phosphatidylethanolamine PE (14:0/14:0), phosphatidylcholine PC (14:0/14:0), phosphatidic acid PA (14:0/14:0), phosphatidylserine PS (14:0/14:0), phosphatidylinositol PI (17:0/20:4), and lysophosphatidylcholine LPC (17:1). Fatty acid standard FA (17:1) was from Nu-Chek Prep (Elysian, MN). UPLC-grade solvents acetonitrile, water, and isopropanol were purchased from Fisher Scientific (Hanover Park, IL). Arachidonic acid, azelaic acid, and S-(5'-adenosyl)-L-homocysteine were purchased from Sigma-Aldrich (St Louis, MO). Adrenic acid was purchased from Santa Cruz (Dallas, Texas). The MS/MS spectra from METLIN⁸ and LipidMaps databases were used as reference spectra for comparison purposes.

Animal Irradiation and Sample Collection

This study was conducted in accordance with applicable federal and state guidelines and was approved by the Institutional Animal Care and Use Committee of the Lovelace Biomedical and Environmental Research Institute (LBERI). Male C57Bl/6 mice (approximately 10–12 weeks old, 25–30 g) were received from Charles River Laboratories (Frederick, MD) and were quarantined for 14 days prior to group assignment by body weight stratification for randomization onto the study. There were eight mice per study group (control vs ⁹⁰Sr) per time necropsy time point (Table 1) for a total of 80 mice.

Animals were administered ⁹⁰Sr intravenously by tail vein injection with 200 ± 0.3 kBq ^{85/90}SrCl₂ solution in a volume of 50 μ L. Strontium-85 (⁸⁵Sr) was used as a tracer for the purpose of measuring strontium whole-body content. Strontium-85 comprised approximately 1% of the total strontium activity.

After $^{85}\text{Sr}/^{90}\text{Sr}$ administration, mice were housed individually in microisolator cages, with lead shielding used to avoid radiation exposure due to cross-irradiation from adjacent mice, which were sources of radiation. All animals had unlimited access to Teklad Certified Global Rodent Diet 2016 (Harlan Teklad, Madison, WI) and water except during dose administration and whole-body *in vivo* counting. No adverse effects to the animals were noted during the course of the study. In addition, no significant changes in food consumption and body weight were noted throughout the 30-day study.

On scheduled necropsy days (4, 7, 9, 25, and 30 days after $^{85}\text{Sr}/^{90}\text{Sr}$ administration), animals were euthanized by intraperitoneal (IP) injection of Euthasol (>150 mg/kg [390 mg/mL pentobarbital and 50 mg/mL phenytoin in sterile saline]) and weighed. Blood was collected at the time of necropsy by cardiac aspiration with a syringe and needle. A maximal blood collection was obtained from each animal and placed into a serum separator tube (BD Microtainer Serum Separator Tube REF365956). The needle was removed prior to placement in the collection tube, that is, the blood was not passed through the needle. The tubes were spun at $1300 \times g$ for 10 min at 4°C . The serum was removed and placed into Eppendorf tubes and stored from -70 to -90°C until analysis.

Dosimetry of ^{90}Sr in Mice

Animals were measured for $^{85}\text{Sr}/^{90}\text{Sr}$ whole-body content using the LBERI *in vivo* photon counting system described previously.⁶ Animals were placed in small containers, with breathing holes, and measured to determine the amount of radioactivity present in each animal daily on days 0–7, then on days 9, 12, 16, 20, 25, 27, and 30 after $^{85}\text{Sr}/^{90}\text{Sr}$ administration (until the time of necropsy). The measurement system was calibrated for different geometries; phantoms representing the animal body and biological samples were developed using a $^{85}\text{Sr}/^{90}\text{Sr}$ NIST-traceable standard solution. Calibration was performed each day prior to the measurement. The animals, samples, and standards were measured for 3 min.

The ^{90}Sr whole-body retention profile was derived from whole-body measurements. The whole-body retention data from each mouse were fitted individually to negative exponential functions. The average values of the parameters of the whole-body retention equation are presented in eq 1:

$$R(t) = 52.1e^{-2.0t} + 20.7e^{-0.13t} + 27.2e^{-0.0049t} \quad (1)$$

Where $R(t)$ represents the whole-body ^{90}Sr content at time (t), expressed as percentage of the injected ^{90}Sr activity; and t is in days. The respective biological half-times were 0.3, 5.3, and 139 d.

To calculate the committed absorbed dose to skeleton, the dose coefficient ($\text{Gy}\cdot\text{Bq}^{-1}$ of administered activity) was derived using eq 2. The comparison between the whole-body activity and the ^{90}Sr content in skeleton at sacrifice time shows that about 95% of the whole-body activity was located in skeleton for all time periods. Therefore, the retention parameters of eq 1 were used to calculate the total number of nuclear transformations ($\text{Bq}\cdot\text{s}$) in skeleton for each time period of the study. The S value ($\text{Gy}/\text{Bq}\cdot\text{s}$) used in eq 2 was derived specifically for young adult mice and rats by Stabin et al.⁹ The dose coefficients ($\text{Gy}\cdot\text{Bq}^{-1}$ of administered activity) for the various time periods used in this study are presented in Table 1.

The committed absorbed doses to the skeleton for each animal were calculated by multiplying the dose coefficient ($\text{Gy}\cdot\text{Bq}^{-1}$) related to the specific sacrifice time for each animal in the

study by the administered activity (Bq). The average committed absorbed doses to skeleton for each time period are presented in Table 1:

$$\frac{D_T}{A} = \int_{t_0}^{t_0+t} \tilde{A}(s) \times S(r_T \leftarrow r_S, t) \left(\frac{\text{Gy}}{\text{Bq}} \right) \quad (2)$$

Where $\tilde{A}(S)$ is the time-integrated activity ($\text{Bq}\cdot\text{s}$), equal to the total number of nuclear transformations in the source region (skeleton); $S(r_T \leftarrow r_S, t)$, in Gy per $\text{Bq}\cdot\text{s}$, is the S value from r_S to r_T of $^{90}\text{Sr} + ^{90}\text{Y}$, where the S value for a given source (r_S)–target (r_T) pair is the mean absorbed dose to the target organ per $^{90}\text{Sr} + ^{90}\text{Y}$ total number of nuclear transformations in the source region.

While the total amount of ^{90}Sr injected into each mouse was 200 kBq, which is equal to 5.4 μCi per mouse, we made the following assumptions in determining that the chemical effect of ^{90}Sr would be negligible to the existing physiological serum concentration of calcium in the experimental mice: (1) assuming that the ^{90}Sr is carrier-free, the injected mass was calculated to be 38 ng ^{90}Sr per mouse, and (2) assuming that initially all the ^{90}Sr was in the plasma, this resulted in a molar amount of 0.42 nmol in plasma. Thus, the serum concentration of ^{90}Sr was 0.21 nmol/mL, while the Ca^{2+} concentration in plasma was 2.36 $\mu\text{mol}/\text{mL}$.¹⁰ Thus, the ratio of Sr/Ca is then 9×10^{-5} or 90 ppm. For bone, the comparison is even more stark. According to Tordoff et al., there is about 480 mg of Ca^{2+} in the mouse skeleton compared with the 38 ng of ^{90}Sr injected. Hence, the Sr/Ca mass ratio is 7.9×10^{-8} or 79 ppb in this study.

Sample Preparation and Mass Spectrometry Analysis

Serum samples were prepared as described in our previous work.⁵ Briefly, one part serum was added to four parts of a chilled chloroform and methanol mixture (2:1, v:v) containing lipid standards at predetermined concentrations, which allowed for determination of appropriate standard curves.⁵ At least one standard per lipid class was included in a cocktail of standards spiked into each sample. Samples were then centrifuged at $13\,000 \times g$ for 5 min to separate the polar and nonpolar species. The upper aqueous phase containing primarily polar metabolites was saved for future detailed metabolomic analysis. The lower phase was collected for lipidomic analysis. The pooled control serum samples containing internal standards were processed via UPLC–MS at every seven injection-intervals as QC samples. The linearity between peak area and concentration in the serum matrix was established by calculating standard curves for two-fold serial dilutions of the spiked internal standards for each class of lipids in the concentration range of 1–350 $\mu\text{g}/\text{mL}$.⁵ The standard curve formulas were then used to determine the relative abundances of lipids in each electrospray ionization (ESI) mode.

Mass Spectrometry Analysis

The lipidomic analysis was performed as described in our previous work.⁵ Briefly, a 2 μL aliquot of each sample was injected into a CSH C18 column $150 \mu\text{m} \times 100 \text{mm}$ (Waters Corp, Milford, MA) with the H-class UPLC Acquity with solvent A (50% acetonitrile with 0.1% formic acid and 10 mM ammonium formate) and solvent B (isopropanol/acetonitrile (90:10 v:v) with 10 mM ammonium formate). The gradient started with 60% solvent A at 0.45 mL/min for the initial 8 min, then switched to 100% solvent B for 1 min, and back to 60% solvent A for the remaining 2 min of the 11 min long gradient.

The Xevo G2-S QToF mass spectrometer was operated in positive (ESI⁺) and negative (ESI⁻) modes over a mass range of 50–1200 Da in two channels, MS and MS^E. The low energy MS channel was operated at 10.0 eV of collision energy, while the MS^E channel included an energy ramp of 10–50 eV. The lock-spray consisted of leucine-enkephalin (556.2771 [M + H]⁺ and 554.2615 [M - H]⁻). The MS data were acquired in centroid mode and processed using MassLynx software (Waters Corp, Milford, MA), as described in the following.

Statistical Analysis and Metabolic Pathway Analysis

As described previously,¹¹ MarkerLynx software (Waters Corp, Milford, MA) was used to deconvolute the data. To determine the peak areas of internal standards, QuanLynx (Waters Corp, Milford, MA) was used. For analyzing the MS^E data, the high-energy scans (fragments) were aligned with low-energy scans (precursors) in MetaboLynx (Waters Corp, Milford, MA). The high-energy scans were used to detect different classes of lipids as previously described based on identifier fragments of each lipid class.¹² MetaboLynx was also utilized to search for neutral loss of 34 Da for phospholipid hydroperoxide species. This is a simple and efficient method to identify various lipid species since the commercially available methods are limited in scope and costly.¹³ Our in-house statistical analysis program, MetaboLyzr,¹⁴ was used to analyze the data and identify statistically significant ions as described previously.⁵ The ion presence threshold was set at 0.7 in MetaboLyzr in each study group for complete-presence ions. Data were then log-transformed and analyzed for statistical significance via the nonparametric Welch's *t* test statistical hypothesis test (*p*-value <0.03). Partial-presence ions were analyzed as categorical variables for presence status (i.e., nonzero abundance in 70% of samples) via Fisher's exact test (*p*-value <0.05). The log-transformed data for statistically significant complete-presence ions were then utilized for principal component analysis (PCA).

Statistically significant ions were putatively identified in MetaboLyzr, which utilizes the Human Metabolome Database (HMDB), LipidMaps, and the Kyoto Encyclopedia of Genes and Genomes (KEGG) database¹⁵ while accounting for possible adducts, H⁺, Na⁺, and NH₄⁺ in the ESI⁺ mode, and H⁻ and Cl⁻ in the ESI⁻ mode. The *m/z* values were compared to the exact mass of small molecules in the databases, from which putative metabolites were identified with a mass error of 20 ppm (ppm) or less. KEGG annotated pathways associated with these putative metabolites were also identified. We also used Metscape (version 2.3.1), which is a plug-in for Cytoscape (version 2.8.2), a visualization software for complex networks. The raw data files containing *p*-value, log fold-change, and KEGG IDs were uploaded into the software, and the compound-interaction network was selected to visualize the statistically significant nodes and edges. The low- and high-energy scans in MS^E mode were used to align key identifier fragments of different classes of lipids within defined retention time windows and compare against fragmentation patterns in online or in-house database.

RESULTS

We detected over 5000 spectral features in the *m/z* range of 200–1200 Da in positive and negative ESI modes combined. The data matrix was organized into five ⁹⁰Sr-exposed groups based on days postexposure and cumulative average skeleton dose, each with a corresponding control group as shown in

Table 1. Each control and ⁹⁰Sr-exposed group included eight mice. Our initial statistical analysis on the overall serum lipidomic profile of mice exposed to ⁹⁰Sr and that of control mice were conducted in Random Forests (RF). The results showed clear separation between the lipidomic profile of the control and the ⁹⁰Sr-exposed mice, with better than 80% accuracy in assigning the top 100 most variable ions to their corresponding time/dose point group. Figure 1 depicts that the

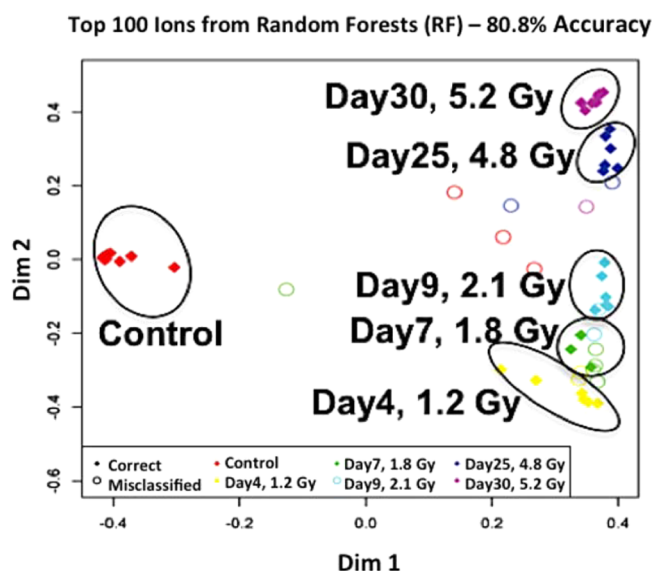


Figure 1. MDS plot created in RF. RF, a machine-learning algorithm, identified the most important variables as those highly ranked on the variable importance report (ntree: 10 000). RF was executed in R software environment, and the variable importance measure was used for ranking, with 25 independent RF models. The bootstrapping of the results along with out-of-bag (OOB) data were then used to calculate the prediction accuracy. The resulting MDS plot here shows the separation of the serum lipidome of control mice from that of ⁹⁰Sr-exposed mice on the first dimension. The individual ⁹⁰Sr-exposed groups separate based on necropsy day/skeleton dose on the second dimension. The accuracy of assigning ions based on relative abundance to the correct study group was better than 80% as shown in this plot.

separation of the lipidomic profile of the ⁹⁰Sr-exposed mice from that of the control mice was achieved in the first dimension of the MDS (multidimensional scaling) plot, while the separation of the lipidomic profiles with the ⁹⁰Sr-exposed group based on time/dose was achieved in the second dimension of this plot (ESI⁺ mode data shown). This indicates that the separation of the lipidomic profiles within the ⁹⁰Sr-exposed groups is secondary to the strong separation observed between the control and the ⁹⁰Sr-exposed groups. Additional RF analysis showed gross and persistent decreases in the serum levels of majority of the 100 highest ranked variable ions (Supplemental Figure 1, ESI⁺ mode data) post ⁹⁰Sr-exposure, which was later confirmed in our subsequent statistical analysis in MetaboLyzr.

MetaboLyzr was ultimately employed for a more detailed statistical analysis of the data, which indicated that 482 serum ions displayed statistically significant changes determined by Welch's *t* test (*p*-value <0.03) in their serum abundances postexposure in both ESI modes combined. Furthermore, PCA enabled us to quickly assess perturbations in the serum lipidome of mice as the result of internal exposure to ⁹⁰Sr. Each time/dose point showed distinct separation between the serum

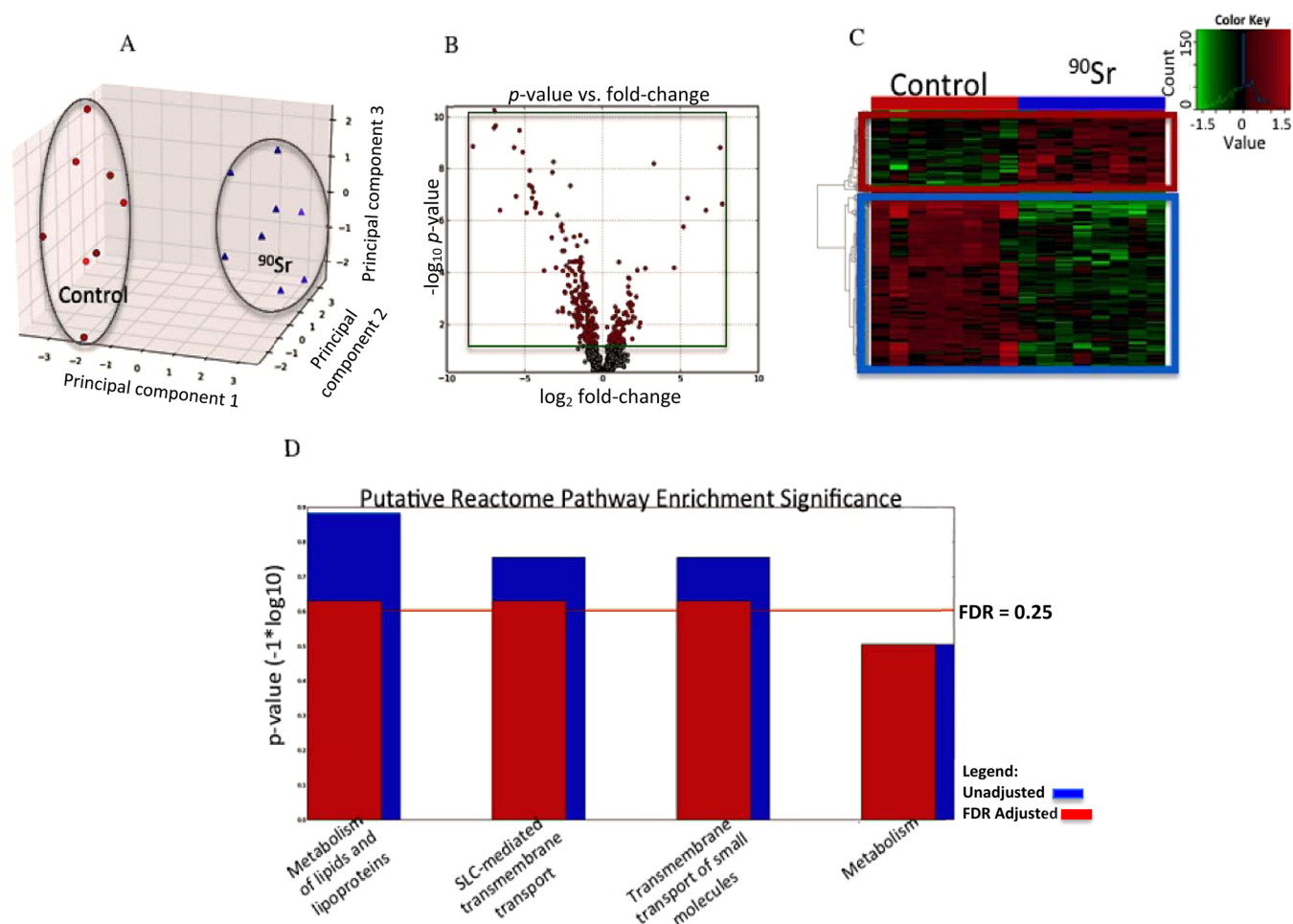


Figure 2. Statistical analysis performed in MetaboLyzer shows distinct differences in the serum lipidome of mice post- ^{90}Sr -exposure. (A) PCA of a separation between the serum lipidome of ^{90}Sr exposed mice from that of control mice at day 9 postexposure at an average cumulative skeleton dose of 2.1 ± 0.32 Gy. (B) The volcano plot shows the individual statistically significant ions in red, which contributed to the separation of the lipidomic profiles of the serum from control and ^{90}Sr -exposed mice in panel A at 9 days postexposure. In this plot, the x -axis is \log_2 fold-change, which shows the direction of the change (negative scale is decrease, positive scale is increase) in the levels of serum ions, while the y -axis is the $-\log$ of p -value, which shows the significance of the change. (C) The heatmap shows ions whose serum abundances changed most statistically significantly postexposure. (D) Pathway analysis plot depicts the Reactome pathways to which the most statistically significant ions were assigned. The orange line is the significant threshold specified on the y -axis by $-\log$ of p -value with FDR correction of 0.25. The blue bars represent the unadjusted and the red bars the FDR corrected values.

lipidome of the ^{90}Sr -exposed and the corresponding control samples. Figure 2, panel A shows an example of this separation at day 9 postexposure at an average cumulative skeleton dose of 2.1 ± 0.32 Gy. The volcano plot in Figure 2, panel B shows the individual statistically significant ions in red, which contributed to the separation of the lipidomic profiles of the serum from control and ^{90}Sr -exposed mice at 9 days postexposure. The y -axis in this volcano plot, $-\log_{10}$ (p -value), indicates the significance of the change in the serum level of the ions, while the x -axis, \log_2 (fold-change), shows the decrease (negative scale) and the increase (positive scale) in the serum levels of ions. As evident from this volcano plot, there are more ions showing statistically significant decreases than increases at day 9 postexposure and average cumulative dose of 2.1 ± 0.32 Gy. This is also observed at other time/dose points throughout the experiment. This suggests that internal exposure to ^{90}Sr causes a persistent decrease in many serum lipids. This decrease is also evident from the heatmap in Figure 2, panel C, with the bottom three-quarters of the heatmap displaying ions with decreasing levels post ^{90}Sr exposure at study day 9. However, the

attenuation of serum ions was more predominant; there were ions, as seen in the volcano plot and the heatmap, that showed clear increases in their serum levels postexposure. Putative identities were assigned to statistically significant ions, which enabled us to map them out to their associated metabolic pathways. Figure 2, panel D displays the Reactome metabolic pathways with the highest significance to which ions were assigned. The blue and red bars are the unadjusted and the FDR (false discovery rate) adjusted $-\log$ of p -value, respectively, which specifies statistical significance, while the orange horizontal line marks the significance threshold. The putative identities of the ions and the associated Reactome pathways indicate significant changes in the membrane lipids and those involved in transmembrane transport as the result of exposure to ^{90}Sr . This is in line with previous research on radiation-induced lipid peroxidation, which leads to increased membrane permeability¹⁶ and disruption of transmembrane processes,¹⁷ such as transport of small molecules as indicated in our pathway analysis in Figure 2, panel D. To validate the identities of the statistically significant serum ions we used the

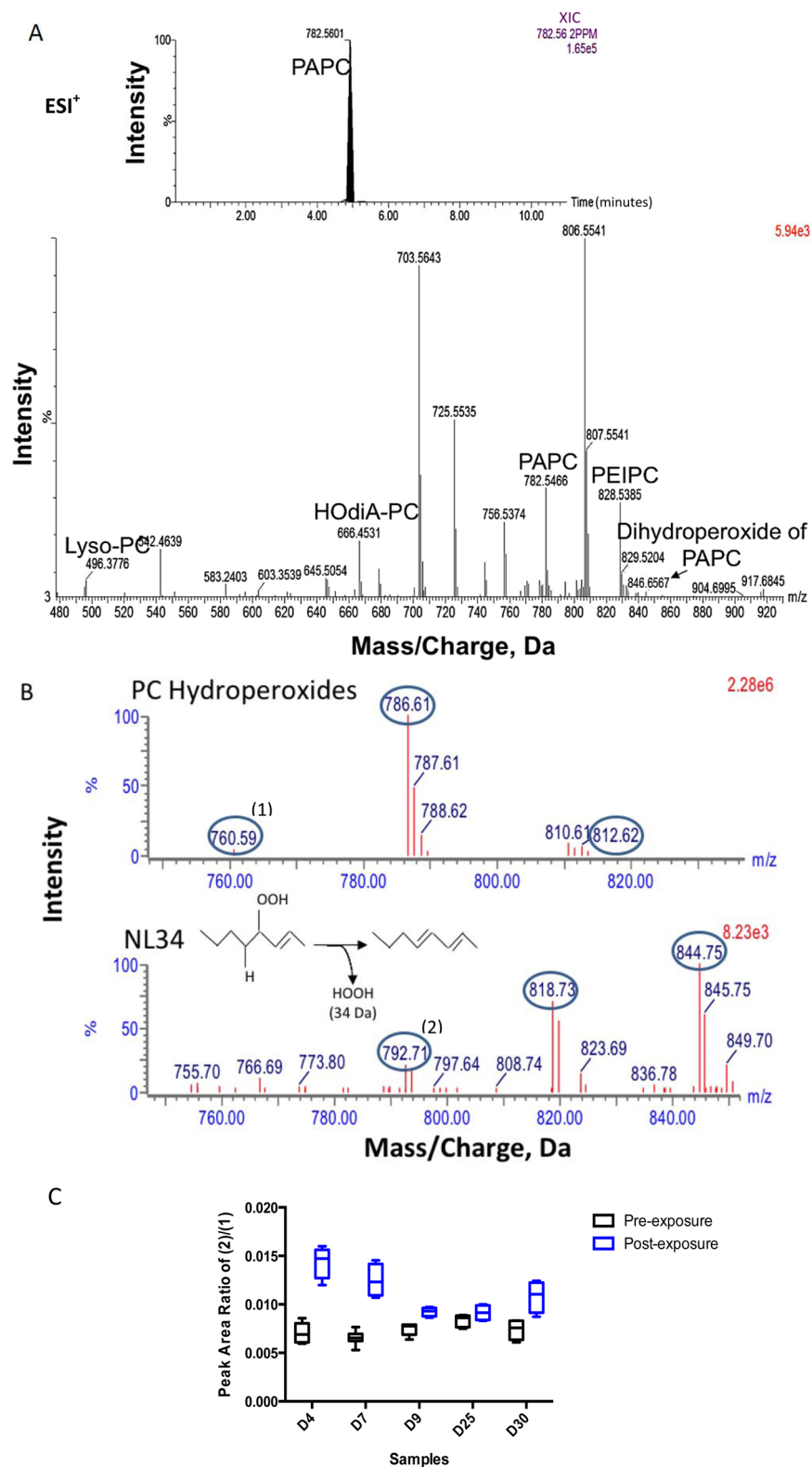


Figure 3. (A) Oxidation of esterified PCs gives rise to a variety of fragmented and nonfragmented species. Top figure shows the precursor PAPA at m/z 782.5601 in an extracted ion chromatogram (XIC) view. This precursor gives rise to multiple products under oxidative stress conditions in ^{90}Sr -exposed mice shown in the lower figure in panel A. The fragmented oxidized species are at $m/z < 782$ and nonfragmented oxidized products at $m/z > 782$. Abbreviations: HOdiA-PC, 5-hydroxy-8-oxo-6-octenedioic acid esters of Lyso-PC; PAPA, 1-hexadecanoyl-2-eicosatetra-5',8',11',14'-enoyl-*sn*-glycero-3-PC; PEIPC, 1-hexadecanoyl-2-(5,6-epoxyisoprostane E2 oyl)-*sn*-glycero-3-PC. (B) Examples of PCs (top spectrum) and their corresponding hydroperoxide species identified by the neutral loss of 34 Da (HOOH). (C) Increase in the ratio of serum abundance (peak area) of hydroperoxide species at m/z 792.71 (2) to that of its corresponding PC (34:1) at m/z 760.59 (1) as the result of ^{90}Sr exposure throughout the course of the study.

LC-MS^E methods described in our previous study⁵ to assign each ion to its appropriate lipid class. We also used the fragmentation pattern of the ions against those in online and our in-house databases to determine the length of the acyl chains.

MS^E is a useful approach to classify lipids based on their identifier fragments and retention time with the help of nonendogenous lipid standards from each lipid class.¹⁸ As shown in Supplemental Figure 2, the low-energy MS scan is aligned with the high-energy scan in MS^E mode containing identifier fragments of each lipid class. For instance, in ESI⁺ mode, the LPCs can easily be mapped to the retention time window of 1.1–1.90 min based on tracing their identifier fragment of m/z 184.07, which is due to the cleavage of the phospho-headgroup. The length of the acyl chains then can be determined by manual examination of the MS/MS data for each LPC species. Supplemental Figures 2A (ESI⁺) and 3B (ESI⁻) show how MS^E data may be utilized to quickly map different lipid classes to their respective retention time window using fragment identifiers of lipid standards. Using this useful and quick approach, we were able to detect several classes of lipids in both ESI modes including PCs, triacylglycerols (TGs), and cholesterol esters (ChoEs), PEs, LPA, and hydroperoxide PCs. Furthermore, serial dilutions carried out using nonendogenous representative of each lipid species serve as a relative quantification approach for the ions of interest. In addition, MetaboLynx (Waters Corp.) was used to search for nonenzymatic oxidation products of lipid species. The nonenzymatic ROS (reactive oxygen species)-mediated oxidation of the esterified acyl chains of PCs, LPCs, and TGs gives rise to an array of oxidized lipid species. Because of the suitability of membrane phospholipids to oxidative fragmentation, the majority of the ions identified here were the truncated oxidized PCs and the resulting fatty acid fragment. For instance, the peak at m/z of 782.5 in Figure 3, panel A identified as palmitoyl-arachidonoyl-phosphatidylcholine (PAPC) was the precursor, which was found to give rise to several oxidative fragmented ($m/z < 782.5$) and nonfragmented ($m/z > 782.5$) products. We used the classical neutral loss scan of 34 Da to search for hydroperoxide species of three of the most statistically significant PCs post ⁹⁰Sr exposure as illustrated in Figure 3, panel B in ESI⁺ mode. Although the serum abundance of these oxidation products of PCs is normally very low, exposure to ⁹⁰Sr induced a slight increase. Panel C in Figure 3 is an example of the increase in the serum levels of a hydroperoxide PC, marked (2), postexposure compared to its corresponding PC, marked (1), in terms of peak area ratio of (2) to (1). At study days 4 and 7, this increase is more evident with the levels subsiding by study day 9 through the end of the experiment.

From the list of statistically significant ions, we were able to identify several ions as LPCs, PCs, PEs, SMs, monoacylglycerols (MGs), diacylglycerols (DGs), ChoEs, and TGs in ESI⁺ (Supplemental Tables 1 and 2) along with hydroperoxide PCs and LPCs using the described methods above. We also identified PSs and FAs in the ESI⁻ mode. From the above list, we focused on a subset of 27 ions that showed the most significant changes in their serum abundances post ⁹⁰Sr exposure. We also chose these ions for further analysis based on their biological role in relation to each other. Table 2 shows the ions that were further analyzed, grouped based on lipid class. While PCs, DGs, and LPCs show early and persistent decreases in their serum levels postexposure, PC hydro-

Table 2. Examples of Statistically Significant Lipids along with Their Fold Changes Throughout the 30-Day Study

	exposure		
	external γ^a	¹³⁷ Cs ^b	⁹⁰ Sr
	1 day postexposure 3.5 Gy	2 days postexposure 1.95 Gy	4 days postexposure 1.21 Gy
TG	–	–	↑
ChoE	–	–	↑
PC	↑	↓	↓
LPC	↑	↑	↓
PE	↑	↑	↓
LPE	–	↓	↓
DG	–	–	↓
SM	↑	↑	↓
palmitic acid	–	↓	↓
linoleic acid	–	↓	↓
arachidonic acid	–	↑	↑
azelaic acid	–	–	↑
adrenic acid	–	–	↑

^aWang, C.; Jun, Y.; Jihua, N. Plasma phospholipid metabolic profiling and biomarkers of rats following radiation exposure based on liquid chromatography–mass spectrometry technique. *Biomedical Chromatography* 2009, 23 (10), 1079–1085. ^bGoudarzi, M.; Weber, W. M.; Mak, T. D.; Chung, J.; Doyle-Eisele, M.; Melo, D. R.; Brenner, D. J.; Guilmette, R. A.; Fornace Jr., A. J. Metabolomic and Lipidomic Analysis of Serum from Mice Exposed to an Internal Emitter, Cesium-137, Using a Shotgun LC–MSE Approach. *J. Proteome Res.* 2014.

peroxides show slight increases in their serum levels postexposure particularly at earlier time-points. This increase is accompanied by an increase in TGs and ChoEs (Figure 4). Furthermore, we detected a slight increase in the serum levels of arachidonic acid, a known inflammation marker, and adrenic acid, which is a metabolic 2-carbon elongation product of arachidonic acid. We also observed a marked increase in the serum levels of azelaic acid post ⁹⁰Sr exposure. Azelaic acid is a 9-carbon diacid, which forms by oxidative cleavage of the 9,10-double bond of the unsaturated fatty acyl chains of phospholipids.¹⁹ The increase in the serum abundance of azelaic acid may serve as yet another evidence for ROS-mediated oxidative stress in ⁹⁰Sr-exposed mice.

To better understand the lipid signaling network, and how these serum perturbations may be explained in terms of cellular metabolic processes, we used Metscape (version 2.3.1), which is a plug-in for Cytoscape, a visualization software for complex networks. This complementary network analysis grouped the statistically significant ions into biological nodes while specifying the relationship between the nodes with arrows (Supplemental Figure 3). The nodes that showed the most significant differences between the serum lipidome of the control and the ⁹⁰Sr-exposed mice were glycerophospholipid metabolism, phosphatidylinositol phosphate metabolism, cholesterol biosynthesis, and bile acid biosynthesis. Changes in these nodes were also positively correlated with those in arachidonic acid metabolism, which is a well-known proinflammatory pathway, and leukotriene metabolism. Perturbations in these metabolic pathways are similar to those reported in previous lipidomic analyses on the effects of external beam as well as internal emitter ¹³⁷Cs on the serum lipidome of mice.⁵

These findings collectively suggest that ⁹⁰Sr-exposure induces gross attenuations in the serum abundances of precursors of

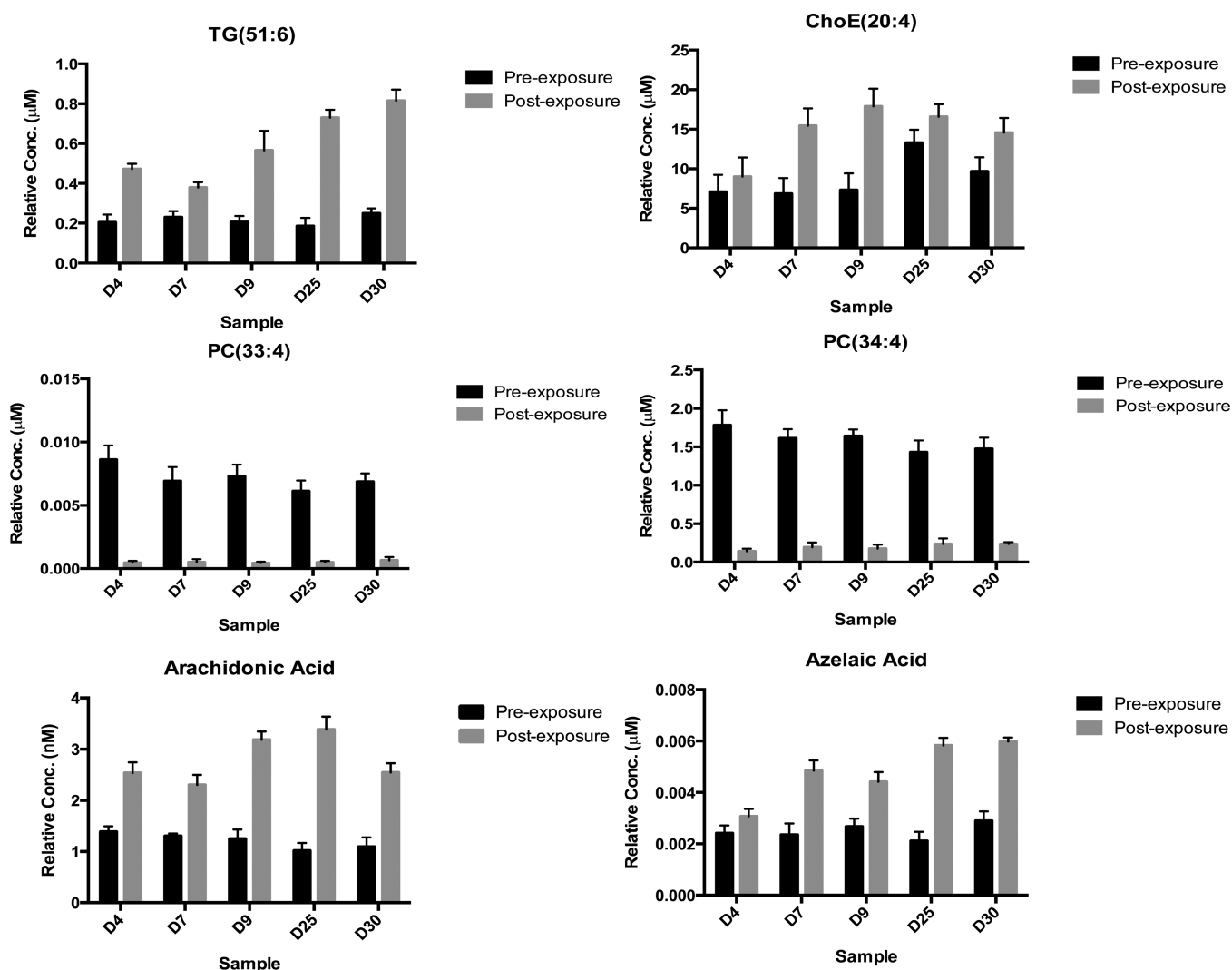


Figure 4. Individual lipids and fatty acids identified as most statistically significant and biologically important post ^{90}Sr exposure in serum. While PCs in this figure show persistent decreases in their serum abundance postexposure, TG, ChoE, arachidonic acid, and azelaic acid show the opposite trend postexposure throughout the course of the 30-day study.

phospholipids such as DGs as well as phospholipids and their associated lipid inflammatory mediators such as arachidonic acid. We also observed a large increase in the levels of TGs and ChoE, which has been reported in previous studies with 6 Gy of external irradiation in rats²⁰ and 5 Gy of whole-body external irradiation in mice.²¹ Although the levels of these lipids reverted back to normal after one radiation exposure, in our current study, the ^{90}Sr exposure-induced increases persisted until the end of the experiment, day 30, at 5.2 ± 0.73 Gy. Although exposure to ^{90}Sr perturbs the serum levels of some the same molecules as does exposure to external γ -irradiation and ^{137}Cs , which decays primarily via emitting γ rays, the levels of these molecules change differently with ^{90}Sr . Table 3 shows a summary of the changes observed in the current study at the average cumulative dose of 1.2 Gy at 4 days postexposure along with those reported in literature for ^{137}Cs ⁵ and external beam γ irradiation.²² The later two cases show similar increases in the levels of LPC, PE, and SM, which is the opposite of what we observed in this study. Both internal emitters, however, show a decrease in the levels of PCs, while an increase was reported with γ irradiation 24-h postexposure. Along with persistent decreases in PCs and LPCs, the finding points to little or no

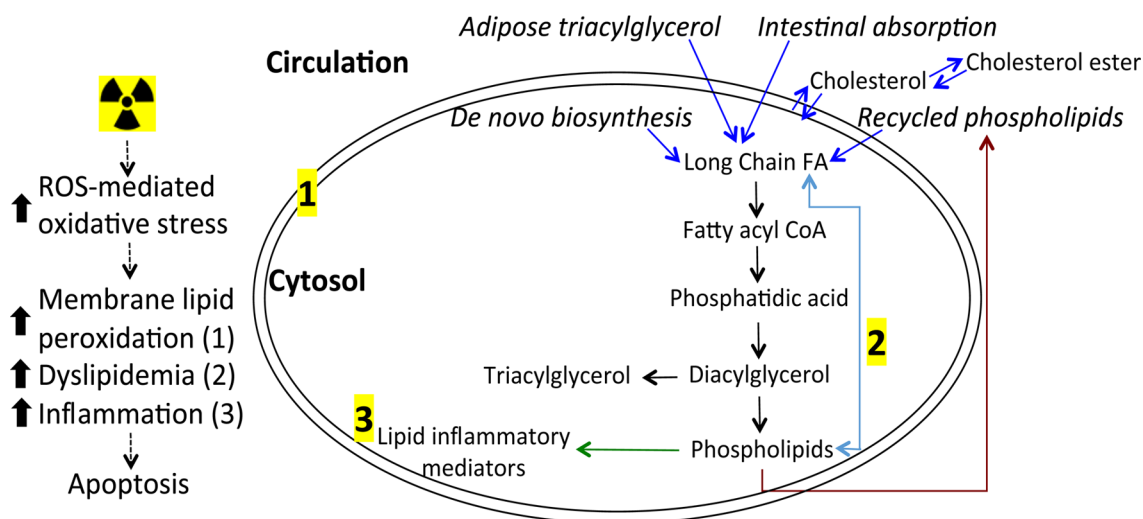
recovery or adaptation during the continued irradiation of the bone marrow and the soft tissues around it. It is possible that the biological lifetime of the end points measured are longer than the experimental time points, leading to an integration of effects from the continuing radiation exposure. This observed perturbation in the serum lipid profile and dyslipidemia post ^{90}Sr exposure strongly suggests an imbalance between circulating and cytosolic fatty acids (Figure 5).

DISCUSSION

In this study, we explored perturbations in the serum lipidome of mice induced by internal exposure to ^{90}Sr . In addition to pivotal structural roles, lipids also play important roles as signaling molecules. They are also major targets for radiation-induced ROS damage.^{23,24} ROS readily interact with reactive methylene hydrogen atom of membrane phospholipids, removing electrons and producing reactive intermediates. This alters the structure and function of critical membrane lipids leading to further cell injury. While perturbation in lipid and energy metabolism is well-documented post external gamma irradiation, this is the first study focused on the effects of internal exposure to a pure beta-emitting radionuclide that

Table 3. Early in Vivo Lipidomic Response in Blood after Exposure to External Gamma Irradiation and Two Internal Emitters, ^{137}Cs and ^{90}Sr

compound	<i>m/z</i> _RT	identifying fragment(s)	error (ppm)	<i>p</i> -value (Welch's <i>t</i> -test)	fold-change				
					D4	D7	D9	D25	D30
LPC16:0	496.339_1.3154	184.07, 478.32, 104.10	9.91	1.90×10^{-03}	1.18	0.80	0.86	0.95	0.94
LPC18:2	520.3388_1.1068	184.07, 502.34, 104.10	1.93	2.60×10^{-03}	0.96	0.66	0.84	0.93	0.96
LPC18:1	522.3545_1.4011	184.07, 504.34, 104.10	1.77	1.70×10^{-02}	0.99	0.89	0.78	0.60	0.87
LPC18:0	524.3705_1.9225	184.07, 506.36, 104.10	1.05	5.70×10^{-03}	0.81	0.93	0.74	0.72	0.70
PC(32:2)	730.5364_4.4757	184.07	2.42	3.80×10^{-03}	0.54	0.32	0.46	0.39	0.61
PC(32:1)	732.5524_4.8745	184.07	1.90	2.80×10^{-02}	0.50	0.31	0.36	0.35	0.52
PC(34:2)	758.5676_5.005	184.07	2.38	3.40×10^{-02}	1.05	1.03	0.90	0.73	0.88
PC(34:1)	760.5837_5.3353	184.07	1.84	2.20×10^{-02}	0.83	0.58	0.57	0.54	0.67
PC(36:3)	784.5838_5.1037	184.07	1.66	3.90×10^{-03}	0.68	0.48	0.53	0.43	0.66
PC(36:2)	786.599_5.4508	184.07	2.20	7.40×10^{-03}	0.78	0.87	0.85	0.64	0.87
PC(36:1)	788.6147_5.7479	184.07	2.17	4.40×10^{-03}	0.73	0.57	0.60	0.33	0.72
PC(34:4)	754.5344_4.8707	184.07	5.00	1.60×10^{-02}	0.13	0.15	0.30	0.30	0.34
PC(33:4)	740.5208_5.0521	184.07	2.27	3.70×10^{-02}	0.07	0.13	0.28	0.19	0.52
SM(38:2)	757.6144_5.3495	184.07	9.74	7.60×10^{-03}	1.88	1.53	1.05	1.34	1.17
TG(56:1)	899.8594_8.4884	NL ^a 271.45, 329.73	14.00	3.28×10^{-02}	2.26	1.84	1.26	1.10	1.21
TG(58:7)	938.8301_8.1381	NL 325.48, 295.38	18.20	9.26×10^{-03}	2.83	4.53	3.10	2.72	2.65
TG(51:6)	854.7287_7.6807	NL 281.21, 351.12	4.77	1.70×10^{-03}	2.32	2.13	1.27	1.15	0.86
TG(61:6)	862.7836_7.7645	NL 273.47, 301.35	4.77	1.84×10^{-02}	3.93	2.05	1.89	1.33	1.13
DG(43:3)	739.6053_2.9561	413.25	7.78	8.15×10^{-03}	0.09	0.05	0.05	0.06	0.07
DG(39:3)	683.5429_2.1702	413.25	4.57	1.40×10^{-02}	0.08	0.05	0.03	0.09	0.07
ChoE(20:4)	673.5909_7.6842	369.36	1.36	1.90×10^{-02}	1.40	1.64	1.89	1.15	1.12
ChoE(18:2)	649.5907_7.7904	369.36	1.72	7.90×10^{-03}	1.28	1.53	1.50	1.17	1.21
arachidonic acid	303.2319_2.3056	259.24	3.46	1.14×10^{-03}	1.81	1.77	2.56	3.12	2.29
palmitic acid	255.2326_2.8714	80.02	1.38	3.24×10^{-02}	1.02	0.55	0.87	0.91	0.81
linoleic acid	279.2328_2.4222	171.43	0.55	4.40×10^{-02}	0.90	0.75	0.72	0.78	1.11
azelaic acid	187.0975_0.5944	97.02	0.41	4.10×10^{-02}	1.30	2.22	2.30	1.64	1.75
adrenic acid	367.2637_2.6308	287.19, 313.17	1.55	2.60×10^{-02}	1.10	1.48	1.28	1.40	1.29

^aNL stands for neutral loss.**Figure 5.** Overall pathway analysis shows the pathways, which played important roles in shaping the lipidomic profile of serum in the ^{90}Sr -exposed mice based on the statistically significant intermediates identified in this study. This figure summarizes all the observed perturbations in the lipidome. Notable features of radiation responses are numerically marked with respect to membrane lipid peroxidation (1), and cytosolic events leading to dyslipidemia (2) and increases in the level of lipid mediators of inflammation (3).

has a significantly nonuniform spatial dose pattern. The results indicate a persistent decrease in the serum abundance of PCs and LPCs as seen in Figure 4 and Table 2. The decrease in PCs is in accordance with what we observed with internal exposure to ^{137}Cs , which may indicate that a decrease in the serum levels of PCs is a general yet strong indicator of radiation exposure-

induced cellular injury. However, in the case of ^{137}Cs exposure, the levels of PCs recovered by the end of the 30-day experiment, while in the current study, such a recovery was not observed. Furthermore, we observed persistent increases in the levels of TGs and ChoEs and a decrease in the levels of DGs. This may be related to the different cell populations being

irradiated, that is, the whole body for ^{137}Cs versus mostly bone and bone marrow cells for ^{90}Sr . This may also be indicative of dyslipidemia as the result of chronic irradiation due to incorporation and retention of ^{90}Sr in the body and the resulting ROS-mediated oxidative conditions. Dyslipidemia is known to be positively correlated with lipid peroxidation induced by ROS-mediated oxidative stress, both of which can lead to cellular dysfunction and apoptosis.²³ The pathway analysis and a decrease in PCs serum levels along with an increase in azelaic acid and PC hydroperoxide species post ^{90}Sr exposure indicate perturbations in membrane phospholipids most likely due to lipid peroxidation. In addition, the increase in triacylglycerols and cholesterol esters indicates dyslipidemia accompanied by an increase in the serum levels of arachidonic acid, an inflammatory marker.

In addition, we detected an increase in the serum levels of arachidonic acid and adrenic acid. An increase in this lipid inflammatory mediator points to proinflammatory cellular response post ^{90}Sr exposure. Such increase was also observed in mice exposed to ^{137}Cs .⁵ Arachidonic acid is released as a free fatty acid upon damage or perturbations to the membrane via several pathways: (a) inflammatory or immunological stimuli, (b) calcium ionophores, (c) irradiation, (d) tumor promoting agents, and (e) mechanical agitation.²⁵ The free arachidonic acid then reacts with prostaglandin cyclooxygenase and is converted into a variety of bioactive products. Therefore, an increase in the serum levels of this fatty acid hints at perturbations in cellular signaling and membrane damage under proinflammatory chronic exposure to ^{90}Sr . Arachidonic acid serum levels in this study rose by dose in this study to more than twice the pre-exposure levels by study day 25, after which a slight decrease in the levels was observed (Figure 4). The increasing arachidonic acid serum level was an expected consequence of exposure to ^{90}Sr due to the resulting oxidative conditions. Moreover, we detected a slight increase in the serum levels of adrenic acid postexposure. Adrenic acid is the 2-carbon elongation product of arachidonic acid, and its increase is associated with that of arachidonic acid.²⁸ Interestingly, we also observed a marked increase in the levels of another fatty acid, azelaic acid, which is a common oxidation product of truncated phospholipids. The resulting phospholipid, hexadecyl azelaoyl-glycerophosphocholine has been associated with tissue injury and apoptosis.²⁶ Although the identity of the resulting phospholipid could not be confirmed in our study, the distinct increase in the serum levels of azelaic acid is another indication of ROS-mediated lipid peroxidation. While arachidonic acid has been reported previously as a potential radiation-induced marker, along with PCs, LPCs, PEs, and SMs as listed in Table 3, the statistically significant elevation in serum levels of azelaic acid seen as early as 4 days post- ^{90}Sr -exposure at the cumulative average dose of 1.2 Gy may be unique to the lipidomic signature of ^{90}Sr .

It has been increasingly recognized that oxidized phospholipids are not only byproducts of lipid peroxidation induced by proinflammatory conditions, but also are important cellular signaling molecules that contribute to initiation and amplification of inflammation. Membrane phospholipids are especially susceptible to ROS-mediated damage and will undergo oxidative fragmentation to form an array of oxidized lipids as seen in Figure 3. Although this phenomenon has been observed in chronic inflammatory microbial infections and diseases,²⁷ this study is the first to identify perturbation of these lipid species in chronic irradiation due to incorporation and

retention of ^{90}Sr into the body. The results of this study strongly suggest perturbations in the lipid metabolism, membrane phospholipids, and free fatty acid metabolism as illustrated in Figure 5. Together, these results paint a unique lipidomic profile for in vivo radiation exposure due to incorporation of ^{90}Sr , which may help in determining exposure in individuals after a nuclear or a radiological event.

CONCLUSION

This study for the first time reports on in vivo effects of internal exposure to ^{90}Sr . ^{90}Sr is the second most feared radionuclide in the fallout and groundshine from a nuclear explosion. Contamination of water and food sources with ^{90}Sr can have devastating consequences for the population in the immediate disaster areas. Continued internal irradiation by ^{90}Sr via ingestion of contaminated water and food in the surrounding areas is also a serious environmental and health hazard, as seen in the recent Fukushima accident. Therefore, it is important to develop exposure assessment diagnostic and monitoring tools specific to ^{90}Sr for immediate and long-term care for the affected populations. The robust serum lipidomic signature for ^{90}Sr exposure reported in this study is an example of how current MS advances can help establish such diagnostic and monitoring clinical measures. The results of this study indicate a decrease in serum levels of PCs, LPCs, and DGs with an increase in TGs and ChoEs. The inflammatory lipid mediators, arachidonic acid, adrenic acid, and azelaic acid, showed statistically significant increases in their serum levels. The changes in the serum abundances of these ions were persistent through the end of the 30-day study. Azelaic acid in particular is an indicator of lipid peroxidation and is formed upon oxidative fragmentation of truncated phospholipids. These results together with an increase in triacylglycerols and cholesterol esters indicate dyslipidemia in the serum of mice internally exposed to ^{90}Sr .

ASSOCIATED CONTENT

Supporting Information

The Supporting Information is available free of charge on the ACS Publications website at DOI: 10.1021/acs.jproteome.5b00576.

Heatmap of persistent statistically significant decreases in intensity of serum ions; alignment of low and high energy scans in MS^E mode; overall pathway analysis of the most statistically significant biological nodes; list of additional ions with statistically significant changes in their serum abundance as early as 4 days postexposure (PDF)

AUTHOR INFORMATION

Corresponding Author

*Phone: 202-687-4324. E-mail: mg668@georgetown.edu.

Author Contributions

All authors participated in preparation of this manuscript and have given approval to the final version of the manuscript.

Notes

The authors declare no competing financial interest.

ACKNOWLEDGMENTS

The authors would like to thank Georgetown University's Radiation Safety Office, and Dr. Amrita Cheema and Kirandeepp Gill at the Proteomic and Metabolomics Shared Resources for their help in this study. The authors would like to also thank James Bulgarelli at Waters Corp. for his advice on using the MS^E approach. This study was supported by the National Institute of Health (National Institute of Allergy and Infectious Diseases) Grant No. U19 A1067773, PI D.J.B., and the Proteomic and Metabolomics Shared Resources, NIH P30 CA51008.

ABBREVIATIONS

strontium-90, ⁹⁰Sr; phosphatidylcholine, PC; lyso-phosphatidylcholine, LPC; triacylglycerol, TG; cholesterol ester, ChoE; sphingomyelin, SM; monoacylglycerol, MG; diacylglycerol, DG; cesium-137, ¹³⁷Cs

REFERENCES

- Goudarzi, M.; Mak, T. D.; Chen, C.; Smilenov, L. B.; Brenner, D. J.; Fornace, A. J., Jr. The effect of low dose rate on metabolomic response to radiation in mice. *Radiat. Environ. Biophys.* **2014**, *53*, 645–657.
- Tyburnski, J. B.; Patterson, A. D.; Krausz, K. W.; Slavik, J.; Fornace, A. J., Jr.; Gonzalez, F. J.; Idle, J. R. Radiation metabolomics. 2. Dose- and time-dependent urinary excretion of deaminated purines and pyrimidines after sublethal gamma-radiation exposure in mice. *Radiat. Res.* **2009**, *172*, 42–57.
- Tyburnski, J. B.; Patterson, A. D.; Krausz, K. W.; Slavik, J.; Fornace, A. J., Jr.; Gonzalez, F. J.; Idle, J. R. Radiation metabolomics. 1. Identification of minimally invasive urine biomarkers for gamma-radiation exposure in mice. *Radiat. Res.* **2008**, *170*, 1–14.
- Coy, S. L.; Krylov, E. V.; Schneider, B. B.; Covey, T. R.; Brenner, D. J.; Tyburnski, J. B.; Patterson, A. D.; Krausz, K. W.; Fornace, A. J., Jr.; Nazarov, E. J. Detection of radiation-exposure biomarkers by differential mobility prefiltered mass spectrometry (DMS-MS). *Int. J. Mass Spectrom.* **2010**, *291*, 108–117.
- Goudarzi, M.; Weber, W. M.; Mak, T. D.; Chung, J.; Doyle-Eisele, M.; Melo, D. R.; Brenner, D. J.; Guilmette, R. A.; Fornace, A. J., Jr. Metabolomic and Lipidomic Analysis of Serum from Mice Exposed to an Internal Emitter, Cesium-137, Using a Shotgun LC-MSE Approach. *J. Proteome Res.* **2015**, *14*, 374–384.
- Goudarzi, M.; Weber, W. M.; Mak, T. D.; Chung, J.; Doyle-Eisele, M.; Melo, D. R.; Brenner, D. J.; Guilmette, R. A.; Fornace, A. J., Jr. Development of urinary biomarkers for internal exposure by cesium-137 using a metabolomics approach in mice. *Radiat. Res.* **2014**, *181*, 54–64.
- Goudarzi, M.; Weber, W. M.; Mak, T. D.; Chung, J.; Doyle-Eisele, M.; Melo, D. R.; Strawn, S. J.; Brenner, D. J.; Guilmette, R. A.; Fornace, A. J., Jr. A comprehensive metabolomic investigation in urine of mice exposed to Strontium-90. *Radiat. Res.* **2015**, *183*, 665–674.
- Smith, C. A.; O'Maille, G.; Want, E. J.; Qin, C.; Trauger, S. A.; Brandon, T. R.; Custodio, D. E.; Abagyan, R.; Siuzdak, G. METLIN: a metabolite mass spectral database. *Ther. Drug Monit.* **2005**, *27*, 747–751.
- Stabin, M. G.; Peterson, T. D.; Holburn, G. E.; Emmons, M. A. Voxel-based mouse and rat models for internal dose calculations. *J. Nucl. Med.* **2006**, *47*, 655–659.
- Tordoff, M. G.; Bachmanov, A. A.; Reed, D. R. Forty mouse strain survey of voluntary calcium intake, blood calcium, and bone mineral content. *Physiol. Behav.* **2007**, *91*, 632–643.
- Laiakis, E. C.; Hyde, D. R.; Fornace, A. J., Jr. Comparison of mouse urinary metabolic profiles after exposure to the inflammatory stressors γ radiation and lipopolysaccharide. *Radiat. Res.* **2012**, *177*, 187–199.
- Berdeaux, O.; Juaneda, P.; Martine, L.; Cabaret, S.; Bretillon, L.; Acar, N. Identification and quantification of phosphatidylcholines containing very-long-chain polyunsaturated fatty acid in bovine and human retina using liquid chromatography/tandem mass spectrometry. *J. Chromatogr. A* **2010**, *1217*, 7738–7748.
- Zschörnig, K.; Schiller, J. A simple method to generate oxidized phosphatidylcholines in amounts close to one milligram. *Chem. Phys. Lipids* **2014**, *184*, 30–37.
- Mak, T. D.; Laiakis, E. C.; Goudarzi, M.; Fornace, A. J., Jr. MetaboLyzr: a novel statistical workflow for analyzing postprocessed LC-MS metabolomics data. *Anal. Chem.* **2014**, *86*, 506–513.
- Kanehisa, M.; Goto, S. KEGG: kyoto encyclopedia of genes and genomes. *Nucleic Acids Res.* **2000**, *28*, 27–30.
- Das, D. K. R.; Chakraborty, A.; Sinha, M.; Manna, K.; Mukherjee, D.; Chakraborty, A.; Bhattacharjee, S.; Dey, S. Modulatory role of quercetin against gamma radiation-mediated biochemical and morphological alterations of red blood cells. *Int. J. Radiat. Biol.* **2013**, *89*, 471–481.
- Kumar, M.; Sharma, M. K.; Saxena, P. S.; Kumar, A. Radioprotective effect of Panax ginseng on the phosphatases and lipid peroxidation level in testes of Swiss albino mice. *Biol. Pharm. Bull.* **2003**, *26*, 308–312.
- Lorzate, M.; Sachsenheimer, T.; Glass, B.; Habermann, A.; Gerl, M. J.; Kräusslich, H.; Brügger, B. Comparative lipidomics analysis of HIV-1 particles and their producer cell membrane in different cell lines. *Cell. Microbiol.* **2013**, *15*, 292–304.
- Chen, R.; Yang, L.; McIntyre, T. M. Cytotoxic phospholipid oxidation products cell death from mitochondrial damage and the intrinsic caspase cascade. *J. Biol. Chem.* **2007**, *282*, 24842–24850.
- Ramadan, L. A.; Shouman, S. A.; Sayed-Ahmed, M. M.; El-Habit, O. H. Modulation of radiation-induced organs toxicity by cremophor-el in experimental animals. *Pharmacol. Res.* **2001**, *43*, 185–191.
- Jo, S. K.; Seol, M. A.; Park, H.; Jung, U.; Roh, C. Ionising radiation triggers fat accumulation in white adipose tissue. *Int. J. Radiat. Biol.* **2011**, *87*, 302–310.
- Wang, C.; Yang, J.; Nie, J. Plasma phospholipid metabolic profiling and biomarkers of rats following radiation exposure based on liquid chromatography-mass spectrometry technique. *Biomed. Chromatogr.* **2009**, *23*, 1079–1085.
- Le Lay, S.; Simard, G.; Martinez, M. C.; Andriantsitohaina, R. Oxidative stress and metabolic pathologies: from an adipocentric point of view. *Oxid. Med. Cell. Longevity* **2014**, *2014*, 1.
- Mishra, K. P.; Dayal, R.; Singh, A.; Pandey, A. Reactive oxygen species as mediator of tumor radiosensitivity. *J. Cancer Res. Ther.* **2014**, *10*, 811–818.
- He, C.; Wu, Y.; Lai, Y.; Cai, Z.; Liu, Y.; Lai, L. Dynamic eicosanoid responses upon different inhibitor and combination treatments on the arachidonic acid metabolic network. *Mol. BioSyst.* **2012**, *8*, 1585–1594.
- Chen, R.; Feldstein, A. E.; McIntyre, T. M. Suppression of mitochondrial function by oxidatively truncated phospholipids is reversible, aided by bid, and suppressed by Bcl-XL. *J. Biol. Chem.* **2009**, *284*, 26297–26308.
- Vercellotti, G. M. Microbes, inflammation and atherosclerosis: will old pathology lessons guide new therapies? *Trans. Am. Clin. Climatol. Assoc.* **2001**, *112*, 215.
- Guijas, C.; Astudillo, A. M.; Gil-de-Gómez, L.; Rubio, J. M.; Balboa, M. A.; Balsinde, J. Phospholipid sources for adrenergic acid mobilization in RAW 264.7 macrophages. Comparison with arachidonic acid. *Biochim. Biophys. Acta, Mol. Cell Biol. Lipids* **2012**, *1821*, 1386–1393.